LWT - Food Science and Technology 176 (2023) 114559

Contents lists available at ScienceDirect

LWT

journal homepage: www.elsevier.com/locate/lwt

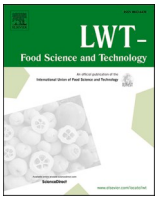

Early identification of mushy Halibut syndrome with hyperspectral image analysis

Samuel Ortega *, Stein-Kato Lindberg, Stein Harris Olsen, Kathryn E. Anderssen, Karsten Heia

Department of Seafood Industry, Nofima AS, P.O. Box 6122, 9291, Tromsø, Norway

ARTICLE INFO

Keywords:
Fish
Greenland halibut
Hyperspectral imaging
Food quality control
Mushy halibut syndrome

ABSTRACT

Mushy Halibut Syndrome (MHS) is a condition that appears in Greenland halibut and manifests itself as abnormally opaque, flaccid and jelly-like flesh. Fish affected by this syndrome show poor meat quality, which results in negative consequences for the fish industry. The research community has not carefully investigated this condition, nor novel technologies for MHS detection have been proposed. In this research work, we propose using hyperspectral imaging to detect MHS. After collecting a dataset of hyperspectral images of halibut affected by MHS, two different goals were targeted. Firstly, the estimation of the chemical composition of the samples (specifically fat and water content) from their spectral data by using constrained spectral unmixing. Secondly, supervised classification using partial least squares discriminant analysis (PLS-DA) was evaluated to identify specimens affected by MHS. The outcomes of our study suggest that the prediction of fat from the spectral data is possible, but the prediction of the water content was not found to be accurate. However, the detection of MHS using PLS-DA was precise for hyperspectral images from both fillets and whole fish, with lower bounds of 75% and 83% for precision and recall, respectively. Our findings suggest hyperspectral imaging as a suitable technology for the early screening of MHS.

1. Introduction

Greenland halibut (*Reinhardtius hippoglossoides*) is a ray-finned fish from the family Pleuronectidae found in the polar regions of the North Atlantic and North Pacific oceans (Herrmann et al., 2013). The Greenland halibut is a flatfish showing ambicolouration, where the eye side (ocular side) has a dark black, brown, or grey coloration, while the blind side is slightly lighter (Barkley, 2015). This species is of commercial interest for fisheries in Canada, Greenland, Iceland, the Faroe Islands, Norway, Russia, and the Barents Sea (Dwyer et al., 2016). In 2020, the total catch volume of Greenland halibut in Norway was approximately 17,000 tons, with an estimated value of 446 million NOK (Fiskeridirektoratet, 2020).

In recent years, there has been an increased awareness in the market since some individuals of Greenland halibut show muscle tissue that is abnormally opaque, flaccid, and jelly-like. These symptoms of the fish muscle are commonly referred to as mushy halibut syndrome (MHS) (Meyers et al., 2019). Although this condition has no negative consequences for human health, the inferior meat quality makes it unattractive for human consumption. The condition is often not discovered until the fish has been filleted. The prevalence of this condition can vary between years and fishing grounds. Nevertheless, significant variations in the quality of landed fish quality can lead to complaints and downgrading of the products on the market (Sogn-Grundvåg & Zhang, 2021). Thus, causing a significant financial loss to the industry. MHS has been poorly investigated in the literature but is hypothesized to be related to nutritional deficiencies (Sydeman et al., 2017).

The main problem with wild fish is that the chemical composition of the muscle, the sensory attributes, and shelf life are highly influenced by preharvest (species, sex, age, feeding, and environmental habits), harvest (fishing tactics and gear choice) and postharvest factors (storage time, temperature) (Alasalvar et al., 2011; Lefevre & Bugeon, 2008; Petricorena, 2015; Sogn-Grundvåg et al., 2022). In the Norwegian whitefish industry, quality defects like parasitic nematodes, residual blood, discoloration, fillet gaping, and soft flesh are registered by labor-intensive procedures, such as candling and manual inspection. It is important to note that candling and manual inspection involve a subjective evaluation and have a high inaccuracy level (Heia et al., 2007). Objective instrumental and chemical methods have been applied to provide information about fish quality. However, these methods are

* Corresponding author.
E-mail address: samuel.ortega@nofima.no (S. Ortega).

https://doi.org/10.1016/j.lwt.2023.114559
Received 11 July 2022; Received in revised form 24 January 2023; Accepted 27 January 2023
Available online 4 February 2023

tedious, complex, time-consuming, and destructive to the product. Thus, these methods have limitations for practical use in the industry (Careche & Barroso, 2009; Careche et al., 2003; Liu et al., 2013; Martinsdttir et al., 2009; Nilsen & Heia, 2009; Nollet & Toldrá, 2009; Olsen et al., 2008). Hence, using an objective and non-destructive instrumental method for rapid tissue analysis would be beneficial.

As far as we are concerned, nowadays, no technology exists for the early screening of MHS. For this reason, in this work, we investigate hyperspectral imaging technology for the non-invasive detection of MHS. Hyperspectral imaging is a non-contact and non-invasive technology able to measure both the spatial and the spectral information of a sample, providing a capability superior to the human eye for characterizing materials. The spectral information is related to the chemical composition and physical structure of the different materials in the sample, as every material produces characteristic light interactions in different spectral bands. Several approaches for measuring hyperspectral images are distinguished by how the light interacts with the material. In a diffuse reflectance illumination scheme, the light is reflected on a surface and is then measured by a hyperspectral camera. In diffuse reflectance, only the spectral features of the surface can be measured. Such surface information is usually insufficient for analyzing the composition of complex and inhomogeneous samples (Wold et al., 2006; Wu & Sun, 2013). Alternatively, using interactance illumination (also known as transflectance), the light is able to penetrate the sample, and it is measured after different internal scatterings have occurred inside the sample (Sivertsen et al., 2009).

Hyperspectral imaging and image analysis techniques have been proven effective technology for non-invasive food safety inspection (Saha & Manickavasagan, 2021, 2021zdoğan et al., 2021). Some examples of successful applications of this technology are the estimation of the chemical composition of cured pork (Ma et al., 2019), the classification of different types of cheese (Lei et al., 2019), or the evaluation of ripeness in agricultural products (Pu et al., 2019), among others. Hyperspectral image technology has been extensively investigated in the literature for the quality determination of seafood products (Ortega et al., 2022). Several research studies have focused on the non-invasive determination of the chemical composition since they are used as indicators of their overall quality or nutritional value. Some examples are the estimation of fat and moisture in Atlantic Salmon (Dixit & Reis, 2023; Zhang et al., 2020; Zhu et al., 2014) or the quantification of the blood content in whitefish (Skjelvareid et al., 2017). Hyperspectral image analysis has also been successfully demonstrated in the literature for the estimation of other quality parameters, such as freshness (Cheng et al., 2014, 2017; Khoshnoudi-Nia & Moosavi-Nasab, 2019; Sivertsen et al., 2011; Yu et al., 2021), the texture (Khoshtaghaza et al., 2016; Q. X. Wang et al., 2021; X. Wang et al., 2019), or the detection of nematodes (Sivertsen et al., 2012).

Other technologies could also be suitable for the detection of MHS. A cheaper alternative to hyperspectral imaging is basic NIR spectroscopy (ElMasry & Wold, 2008). Like hyperspectral imaging, it is non-invasive and rapid, but it is a point measurement such that the measurement is more vulnerable to heterogeneities throughout the fish. Similarly, Raman spectroscopy is another non-invasive technique to measure fat and water content, but like NIR, it is a point measurement and suffers from lower signal-to-noise, such that measurements take longer and are more prone to error (Afseth et al., 2005). Nuclear magnetic resonance is a possible alternative method to detect the syndrome. The method is non-invasive and can provide reliable quantification of water and fat in samples (Jepsen et al., 1999). However, equipment large enough to handle whole fish tends to be expensive, and measurements tend to be relatively slow (10–20 s), so it is unsuitable for high-throughput environments such as fish processing plants. The advantage of hyperspectral imaging over other technologies for this application is its ability to measure the spectral information with high throughput and the possibility to measure the spectral information in for the complete sample. The high throughput will make this technology a valid option to be integrated in a fish production facility in industrial conditions, while the possibility of measuring the spectral variations within the complete sample (not only in specific locations of the sample) would make it possible to identify the MHS event if it is only manifested in certain locations of the fish.

The main goal of this research is to investigate if hyperspectral image technology could be used to detect Greenland halibut affected by the MHS. To this end, we followed two different approaches. First, we investigated if some of the chemical constituents of the fish (water and fat) can be estimated from the spectral data by using constrained spectral unmixing. Secondly, we targeted the automatic identification of fish affected by MHS using supervised classification techniques.

2. Materials and methods

2.1. Sample description

Greenland halibut for this study were caught in the period from September 30th to October 2nd (2021) between 400 and 1500 m depth by a North Atlantic commercial trawler (M/Tr Havtind, length 59.75 m, BT 1860; HP 6100) in the West Greenland Exclusive Economic Zones (EEZ), at the Northwest Atlantic Fisheries Organization (NAFO) divisions 1CD (64°11N-64°29N, 054°46W-055°51W).

The fish were slaughtered, gutted, and their head removed. In an initial screening of the samples by the crew members on board the trawler, sixty-two Greenland halibut (2–3 kg) were collected from eight different trawl hauls. Thirty-five fish were not affected by MHS, and twenty-seven were visually evaluated as presenting MHS. All fish was frozen pre-rigor in blocks (25 kg) in plate freezers and finally stored (<−20 °C). After landing the catch, the frozen samples (n = 62) provided by Lerøy Havfisk LTD (Ålesund, Norway) were transported to Nofima LTD (Tromsø, Norway), where the fish were thawed before being scanned with hyperspectral imaging.

To the best of our knowledge, there are no previous works where the presence of MHS has been related to the fish's chemical composition. For that reason, loin sections (of about 200 g) from 23 out of the 62 samples (11 with no MHS and 12 affected by MHS) were sent for biochemical analysis (Tos Lab AS, Tromsø, Norway) to quantify the contents of water, fat, protein, and ash. Biochemical determination was performed following methods described by the Nordic Committee on Food Analysis (NMKL) and Norwegian Standards (NS). The gravimetric determination of water content was performed with the NMKL 23 method, which involves drying the samples at 102–105 °C for 16–18 h. The water content was measured as the mass lost after drying the sample. The fat content was determined using the NS 9402 method, where a loin segment is homogenized after removing the skin and the vertebral column, and the fat in the homogenate is dissolved, dried, and weighed. The fat content is then calculated from this weight by a given formula. The protein was determined with NMKL 6, a reference method for the quantitative determination of nitrogen in foods and feeds. This reference method includes block digestion, (semi) automatic distillation and titration, and the conventional Kjeldahl method. Finally, the nitrogen content is multiplied by a factor of 6.25 to obtain the protein content. The NMKL 173 method was used for ash determination, where the samples are dried and ashed to constant weight in a muffle furnace at 550 °C. The ash content of a sample is defined as the inorganic residue of a sample after water, and organic matter have been removed.

Table 1
Summary of the chemical composition of the halibut samples.

	No MHS (N = 11)	MHS (N = 12)	Welch *t*-test
Water (%)	74.99 ± 1.55	78.63 ± 6.81	t = −1.80, p-value = 0.096
Fat (%)	10.88 ± 1.52	7.64 ± 3.95	t = 2.62, p-value = 0.019
Protein (%)	14.10 ± 0.73	12.54 ± 2.26	t = 2.27, p-value = 0.040
Ash (%)	1.03 ± 0.05	1.14 ± 0.11	t = −3.22, p-value = 0.005

Table 1 shows the mean value and the standard deviation of the biochemical components, as well as the results of a Two Sample Welch *t*-test. According to these figures, using a 95% significance level, we argue that the main differences between the two groups are related to fat content, protein, and ash.

Fig. 1 shows the corresponding boxplots for each chemical component. The trend shows that the muscle of individuals with MHS contains more water and lower fat and proteins. The ash content is also higher for individuals with MHS. In Fig. 1c, one can observe an outlier in the chemical composition of one of the MHS samples, where the protein content is lower than the other samples. In the visual examination of the fish, that specific sample was flagged as presenting severe MHS, characterized by an extreme jelly-like flesh.

2.2. Hyperspectral image acquisition

The hyperspectral data were recorded using the Maritech Eye (Maritech Systems AS, Molde, Norway), an industrial hyperspectral imaging system. The Maritech Eye is composed of an interactance illumination system and a hyperspectral camera. As argued in the Introduction, the interactance illumination allows the measurement of absorption and scattering properties of the internal layers of biological tissues.

The Maritech Eye interactance illumination consists of two focused halogen light lines inspired by the illumination described in previous research work (Washburn et al., 2017). The light lines are generated by different halogen lamps (900 W of electrical power) and delivered through fiber optic light guides to two cylindrical lenses that generate the parallel and focused halogen light lines. The camera field of view is placed in the middle of these halogen lights. The hyperspectral camera is a HySpex Baldur V–1024N (Norsk Elektro Optikk AS, Oslo, Norway), a pushbroom camera covering the spectral range from 485 to 960 nm with a spectral resolution of 5.5 nm (88 bands) and 1024 spatial pixels. We used a binning of 4 × in this experiment, resulting in 256 spatial pixels per line. The field of view is approximately 300 mm at a working distance of 1000 mm. As it is a pushbroom camera, only the spectral information of a single narrow spatial line is captured by each frame. The remaining spatial dimension is collected by scanning the target sample using a conveyor belt to create a hyperspectral cube. The speed of the conveyor belt was set to 400 mm/s, which is an adequate speed for industrial inspection in the seafood industry. With this setup and an exposure time of 1.9 ms, the final pixel size of the measurements was approximately 1.17 × 0.76 mm.

The aforementioned configuration for the instrumentation results in non-square pixels. There are two options for measuring a hyperspectral image with square pixels: slow down the conveyor belt speed, or reduce the exposure time. On the one hand, in this experiment, the conveyor belt speed was intentionally fixed to match the standard speed for industrial inspection in the seafood industry. On the other hand, decreasing the exposure time negatively impacts the signal-to-noise ratio of the recorded data and hence can compromise the subsequent data analysis. Therefore, since the non-square pixels will not affect the mean spectra of large sample areas, we decided to use this configuration for the measurements.

In order to take into account the color variation within the halibut skin, scans were performed on both sides of the whole fish. After scanning both sides of the whole fish, the fish was filleted and scanned again. In summary, four hyperspectral images were acquired for each halibut using this instrumentation: one image from each side of the whole fish (ocular side and blind side) and one image for each fillet (two fillets per sample). The images of the fillets were measured from the flesh side.

2.3. Hyperspectral image processing

The image analysis proposed in this work is shown in Fig. 2. This workflow was applied independently to both the whole fish and the fillet hyperspectral images. In this work, we targeted two different goals. Firstly, we sought to estimate the biochemical composition of the different halibuts by using constrained spectral unmixing, specifically the fat and water content. The second goal was to automatically identify Greenland halibut affected by the MHS by exploiting their spectral information.

After hyperspectral image acquisition, the images underwent a standard flat field calibration using white and dark references. The

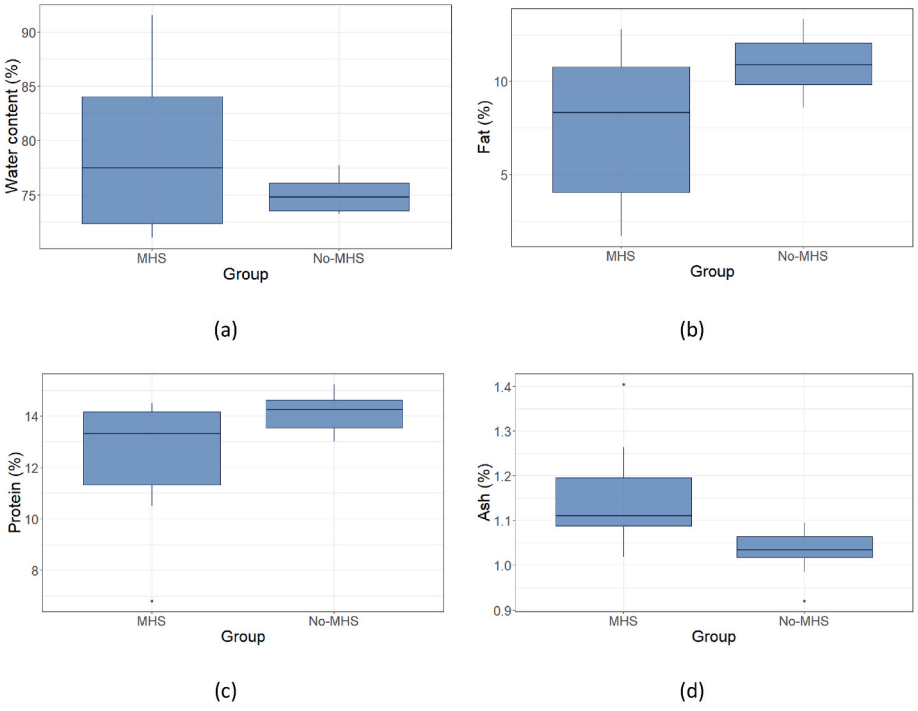

Fig. 1. Boxplots corresponding to the different biochemical components in halibut samples. (a) Water content (b) Fat content (c) Protein content (d) Ash content.

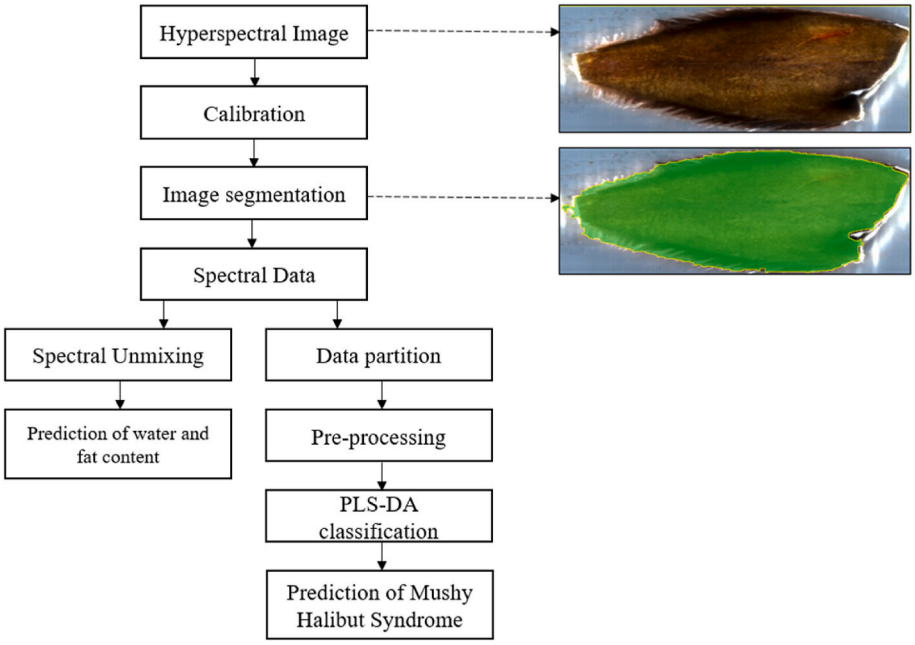

Fig. 2. Flowchart describing the image processing approach.

white reference was taken from a PTFE (Teflon) target plate of 25 mm thickness. A reflectance peak of 95% characterizes the diffuse reflectance of the PTFE target at 410 nm with a monotonically decreasing trend with wavelength, presenting approximately 80% reflectance at 1000 nm (Tsai et al., 2008). The dark reference was captured with the camera lens blocked. After the flat field calibration, the images were segmented to separate the pixels into two classes: those that belong to the background (corresponding to the conveyor belt) and those corresponding to the fish sample. Then, two different branches to process the images were proposed.

In Section 2, we analyzed the differences in chemical composition between individuals affected or not by the MHS. Motivated by those chemical differences, we proposed to investigate if it is possible to estimate the chemical composition of the Greenland halibut from their spectral data. To this end, we explored the use of constrained spectral unmixing. The use of constrained spectral unmixing for estimating chemical compounds in fish samples was previously demonstrated to be accurate for the quantification of the concentration of blood in cod fillets (Skjelvareid et al., 2017). The spectral mixing model is inspired by the interaction between light and matter, and assumes that the measured spectrum in each pixel of a hyperspectral image can be modeled as the linear combination of pure spectra of components, weighted by their relative abundance. The pure spectral components are called endmembers, and the constrained spectral unmixing model aims to estimate their abundances for each pixel of the hyperspectral image. In this work, the endmembers corresponding to blood constituents (oxygenated hemoglobin, deoxygenated hemoglobin, and methemoglobin), fat, and water were used for the spectral mixing model. The absorption spectra of water, lipids, and hemoglobin in its different oxygenation states in the visible and near-infrared regions of the electromagnetic spectrum have been widely characterized in the literature (Khodabux et al., 2007; Wilson et al., 2015). In the spectral region we used in this experiment (486–960 nm), the main absorption peaks are related to oxygenated hemoglobin (543 and 577 nm), deoxygenated hemoglobin (556 nm), and lipids (930 nm). The absorption peak of water (970 nm) is beyond the spectral region covered by our instrumentation. However, there are other spectral features of water in the visible spectral range (Pope & Fry, 1997). In addition to these endmembers, a second order polynomial term was included in the linear mixture model to consider the effects of the light scattering in tissue. In this work, we evaluate the use of constrained spectral unmixing for estimating fat and water from the hyperspectral images of Greenland halibut.

Secondly, the goal was to predict if a sample is affected or not by the MHS from the spectral data information. To this end, a supervised classification approach is followed, where the spectral features extracted from the sample were used as predictors. In this case, the classification problem is binary, and the classes describe whether a sample is affected by the MHS. We used Partial Least-Squares Discriminant Analysis (PLS-DA) to perform the classification.

A data partition strategy was followed to address the classification performance evaluation adequately. The dataset ($n = 62$) was split into three disjoint sets: train, validation, and test. The training samples were used for the PLS-DA modeling, while the validation set was used to evaluate the model performance when different types of pre-processing techniques, different spectral regions, and the different number of components for the PLS-DA modeling were used. Finally, when the optimal combination of these parameters was found for the validation set, the test samples were used to measure the classification performance. The evaluation metrics for the supervised classification were overall accuracy, precision, and recall. The overall accuracy is the rate of correctly classified instances in the entire dataset. High precision indicates the ability of the classifier to avoid the prediction of false positives, while high recall indicates the capability of the classifier to avoid the prediction of false negatives. In this context, a false positive means that the classifier detects MHS in a sample without MHS, while a false negative means that the classifier cannot detect MHS in an affected sample.

The image analysis in this work was performed using the Breeze software for hyperspectral image analysis (Prediktera AB, Umeå, Sweden).

3. Results

3.1. Estimation of the chemical composition using spectral unmixing

In Section 2.1, we demonstrated that the Greenland halibut's chemical composition could be used to differentiate between individuals affected or not by the MHS. In this section, we evaluate whether some of the Greenland halibut's chemical constituents can be estimated non-invasively using hyperspectral image analysis and constrained spectral

unmixing. We used 23 samples for this analysis. In this case, only the water and fat content were estimated using this methodology, as the pure absorption spectra (endmembers) for protein and ash are not available in the literature. As stated in Section 2.3, the spectral linear model used in this study assumes that the endmembers (pure elements) forming the spectra of a Greenland halibut are the main blood constituents (oxygenated hemoglobin, deoxygenated hemoglobin, and methemoglobin), fat, and water. The constrained spectral unmixing was applied to the three types of images available: whole fish (ocular side and blind side) and fillets.

In this study, we were interested in analyzing the strength of the relationship between the reference chemical composition values of the samples and the abundance estimation using constrained spectral unmixing. To evaluate this relationship, we used Pearson's correlation and the 95% confidence interval of Person's correlation since a wide confidence interval indicates that it is impossible to extract robust conclusions about the strength of the relationship between the variables (Schober et al., 2018). The relationship between the chemical composition of the samples and their estimations using constrained spectral unmixing is shown in Table 2. We found a moderate positive correlation for the estimation of water using the spectral data extracted from the fillets, and a strong positive correlation for the fat estimation from the spectral data of both fillets and whole fish (blind side). As already mentioned, a wide 95% confidence interval indicates no evidence to support the strength of the correlation between the estimation of the chemical composition and its actual value. The 95% confidence interval was found wide for the water estimation of whole fish (both ocular side and blind side) and the fat estimation of the ocular side. For this reason, the estimation of water for whole fish (both sides) and fat estimation for the ocular side cannot be considered relevant.

In addition to calculating correlation coefficients, we represented the measured chemical composition and the estimations calculated from the constrained spectral unmixing models using scatterplots in Fig. 3. We also included the 95% confidence ellipses to provide a graphical intuition about the relationship between the variables, i.e., reference data and estimations. These ellipses can be interpreted as confidence areas where the data lie with a certain confidence level. Furthermore, the ellipses can be used as a visual indicator of correlations, being less eccentrical when the variables under study are uncorrelated. Although we found some data samples outside the 95% confidence ellipses, most of the data is within those ellipses. These graphical representations are coherent with the conclusions extracted from the correlations shown in Table 2. In Fig. 3, it is possible to observe that the ellipses corresponding to the estimation of fat are more elongated than those corresponding to the estimation of water, suggesting a stronger correlation for the fat estimations. Similarly, the ellipses corresponding to the fillet estimations are more elongated than the ellipses corresponding to whole fish. Finally, an example of uncorrelated variables can be observed in the estimation of water using the hyperspectral data from the ocular side (Fig. 3a), which is revealed by the circular shape of the 95% confidence ellipse.

In summary, two major trends can be observed in the results for the estimation of the chemical composition (water and fat) of Greenland halibut using constrained spectral unmixing. First, there is a difference in the correlation coefficient between the different types of images, where a lower correlation is found when the linear unmixing is applied to whole fish (both ocular and blind side) compared to fillets. Second, the correlation coefficient for estimating fat abundance is higher than the correlation for water abundance.

Table 2
Pearson correlation and 95% confidence intervals (CI) for the chemical composition of Greenland halibut and abundances from the constrained spectral unmixing model.

Chemical component	Type of image	'Pearson's correlation	'Pearson's correlation 95% CI
Water	Ocular side	0.019	(-0.396, 0.427)
	Blind side	0.519	(0.136, 0.767)
	Fillet side	0.602	(0.378, 0.760)
Fat	Ocular side	0.642	(0.313, 0.834)
	Blind side	0.747	(0.484, 0.886)
	Fillet side	0.812	(0.682, 0.892)

3.2. Detection of MHS based on spectral data

In this section, we present the results of the automatic detection of Greenland halibut affected by MHS by exploiting the spectral information. The number of samples in this study was 62, where 35 were affected by the MHS (56%) and 27 were not affected by the MHS (44%). Therefore, this is a binary classification problem with a balanced dataset, i.e., the number of instances of each class is similar. The classification framework was applied to the three types of hyperspectral images available in the dataset: whole fish (ocular and blind sides) and fillets. The processing framework was performed using the spectral information of the entire sample and the spectral information from a region of interest (ROI) located in the loin of the fish. The data partition was performed by randomly dividing the samples into three independent subsets: training (~73%, 45 samples), validation (~7%, 4 samples), and test (~20%, 13 samples). Different combinations of pre-processing techniques and different spectral regions were evaluated to optimize the classification performance in the validation set. Standard pre-processing techniques for spectral data were evaluated in this study, namely SNV (standard normal variate), centering, and first and second derivatives.

The classification results obtained when applying the processing framework to the samples in the test set are shown in Table 3. The final pre-processing chain selected to generate these results consists of the first derivative of the spectral data followed by centering. Additionally, different spectral ranges were optimal for each type of hyperspectral images. The optimal range for the ocular side classification was found as the combination of the spectral bands from 486 to 588 nm and 907–955 nm. For the blind side classification, this range was 491–659 nm. Finally, the optimal range for the classification of fillets was 486–670 nm. The number of latent variables used in the PLS-DA models was 4, 3, and 5 for the ocular side, the blind side, and the fillets, respectively.

The results of the PLS-DA classification of halibuts with MHS were accurate both for fillets and whole fish. On the one hand, for the fillet samples, all the test set instances were correctly classified (100% of precision and recall). In the fillet samples, using an ROI in the loin part of the sample does not provide any improvement in the classification results compared to using the spectral information from the entire sample. On the other hand, although the classification results for the two types of whole fish images (ocular side and blind side) are precise, the predictions show some false positives and false negatives. We observed an improvement in the classification results in the whole fish samples when the spectral information of the ROI located in the loin of the sample was used. Comparing the results between the classification for the ocular side and the blind side, the results shown in Table 3 suggest that a higher recall characterizes the predictions for the ocular side, while the results for the blind side show higher precision. The interpretation of these results indicates that the PLS-DA model for the ocular side is more likely to produce false positive predictions, while the model for the blind side is more likely to produce false negative predictions. However, the results can be considered promising since the number of misclassifications is low (a single sample in the test set is misclassified for both the ocular side and the blind side).

In Fig. 4 we show some score plots corresponding to the different PLS-DA models, where an intuition about the model behavior can be observed qualitatively. The red color is used for the MHS class and blue for the non-MHS class. These score plots show a clear separation between the two classes under study for all types of hyperspectral images. The latent factors used in these score plots were selected to maximize the

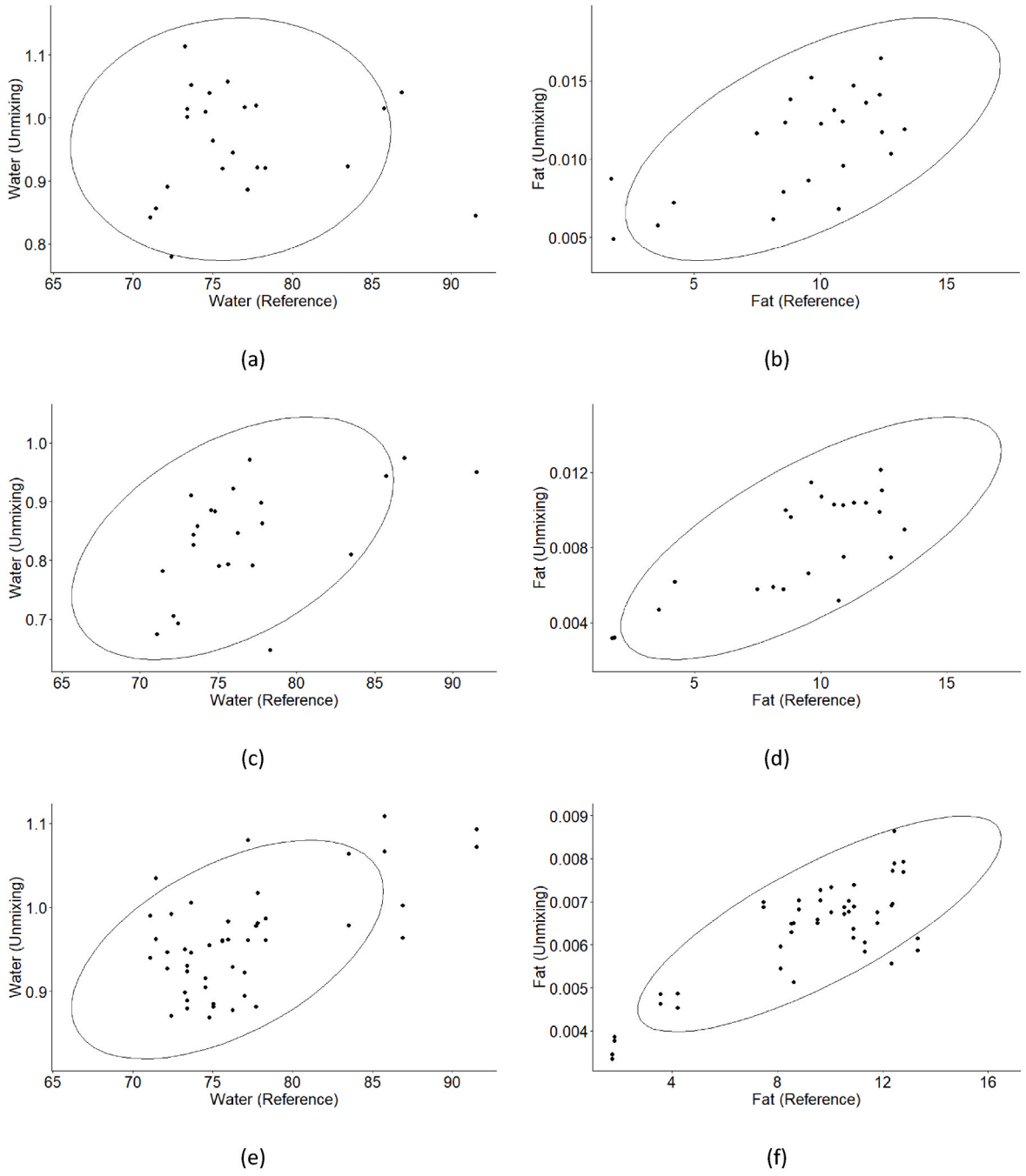

Fig. 3. Scatterplots showing the correlation between the chemical composition and the results from the spectral unmixing model. (a) Water content, ocular side (b) fat content, ocular side (c) water content, blind side (d) fat content, blind side (e) water content, fillets (f) fat content, fillets.

visual clustering between the two classes in a 2-D representation.

In addition, we analyzed the corresponding loadings to provide insights into the PLS-DA models. The loadings are calculated by maximizing the covariance between the projected predictor and response variables and provide information about which variables (in this case which spectral bands) contribute most to the projection to latent variables in the models. In Fig. 5a, we can observe that the most relevant variables for the spectral data from the ocular side are 486 nm (P1 and P2), 492 nm (P3), 513 nm (P3), and 588 nm (P1 and P2). In the case of the spectral data from the blind side (Fig. 5b), the most important spectral bands for the projection are 486 nm (P1 and P2), 492 nm (P2), 513 nm (P2), 524 nm (P2), 545 nm (P2 and P3) and 583 nm (P2 and P3). Finally, for the fillets (Fig. 5c) the most relevant variables are 524 nm (P1 and P2), 540 nm (P4), 545 nm (P2 and P3), 567 nm (P2 and P3), 583 nm (P1 and P2), and 605 nm (P4).

According to the analysis of the PLS-DA models, the spectral information relevant to the identification of MHS is in the visual spectral range, specifically from 486 nm to 605 nm. The most relevant spectral bands differ for the types of hyperspectral images. However, there are some similarities. First, all the models use a spectral feature in the 580–590 nm range. Secondly, the spectral bands 513 nm and 605 nm, used in the models for whole fish and fillets, correspond to the shoulders of the water absorption spectra (514 nm and 605 nm) (Pope & Fry, 1997). The models corresponding to whole fish imaging (ocular side and blind side) share relevant features in the spectral bands 486 nm and 492 nm. Since those bands are not relevant for fillet classification, the spectral features on those wavelengths may be related to the skin, but this fact should be further investigated to be proved. The models

Table 3
Classification results on the test data. TP (true positives), TN (true negatives), FP (false positives), FN (false negatives). Positive class: MHS (n = 6). Negative class: No-MHS (n = 7).

	Whole Fish			ROI Loin		
	Ocular side	Blind side	Fillets	Ocular side	Blind side	Fillets
Accuracy	84.6%	83.3%	**100%**	92.3%	92.3%	**100%**
Precision	75%	83.3%	**100%**	85.7%	**100%**	**100%**
Recall	**100%**	83.3%	**100%**	**100%**	83.3%	**100%**
TP	6	5	7	6	5	7
TN	5	6	6	6	7	6
FP	2	1	0	1	0	0
FN	0	1	0	0	1	0

corresponding to the blind side and the fillets also highlight the spectral features in the bands 540 nm, 545 nm, and 583 nm. Those bands are close to the secondary absorption peaks of oxygenated hemoglobin (543 nm and 577 nm). However, there is no supporting chemical analysis to provide evidence about the relationship of oxygenated hemoglobin and the presence of MHS. Since the MHS is characterized by decoloration in the fish flesh, there may be other specific pigments affecting the spectral signature of the Greenland halibut in the range of 486 nm–605 nm.

Finally, Fig. 6 shows the classification maps when the PLS-DA models are applied to the Greenland halibut hyperspectral images. The hyperspectral images were first divided into superpixels of size 5 × 5 pixels and then the classification was applied to the average spectrum of the superpixels. The results are shown for fillets (Fig. 6a and b) and whole fish (Fig. 6 c-d). The superpixels classified as MHS are represented using red, and the superpixels classified as non-MHS are presented in blue. The white color represents superpixels whose class is uncertain. The percentage of superpixels belonging to each class is also shown as a percentage bar. From these classification maps, it can be observed that the number of superpixels correctly classified is higher for the fillet samples, with a significant difference between the number of superpixels corresponding to each class. In the case of the whole fish classification, the number of superpixel misclassifications is higher.

4. Discussion

In this research work, we have studied MHS, a condition that appears in Greenland Halibut. MHS has no consequences for human health, but the inferior meat quality of fish affected by this syndrome produces a negative economic impact on the fish industry. The research community has poorly investigated MHS, and its causes are still unknown. For this reason, we first analyzed if the chemical composition of the Greenland halibut flesh allowed the differentiation between individuals affected or not by MHS. According to our analysis, the fat content, the protein content, and the inorganic content (measured as the ash content) present statistically significant differences between samples affected or not by MHS. Additionally, we observed that the protein content of a sample showing an extreme jelly-like flesh was much lower than the rest of the samples, which may indicate the relevance of protein deficiency for identifying MHS. Nevertheless, the number of samples (n = 23) used to characterize the differences in chemical composition between the two groups was low, and data from a larger population should be used to reinforce our findings.

Nevertheless, the main goal of this research was to use hyperspectral image technology for the early identification of MHS. Two different alternatives for data processing were proposed to reach this goal. First, we evaluate the estimation of the chemical composition of the Greenland halibut by using constrained spectral unmixing. Secondly, we investigated the use of supervised classification to detect MHS using the spectral data as predictors. In all our experiments, we used three types of hyperspectral images, the two sides of the whole fish before filleting (ocular side and blind side) and hyperspectral images of the fillets.

The first goal of this research was to apply constrained spectral unmixing for the non-invasive estimation of the water and fat content in the halibut samples. The quality of this chemical estimation was quantified by using the Pearson correlation coefficient between the reference chemical composition of the samples and the abundances estimated using the spectral mixing model. The results from this analysis indicate a correlation between the estimated and the actual fat content but not the water content. The low correlation of water estimation can be caused because the spectral range used for the measurements (486–960 nm) does not cover the main absorption peak of water on the near-infrared (970 nm). For this reason, the quality of the water content estimation could be improved if an extended spectral range is used for the hyperspectral sampling.

Additionally, the estimation of the chemical content showed higher correlations for the images from the fillets compared to the whole fish images. This may be due to the optical properties of the skin. We hypothesize that the skin attenuates the light from the sample and weakens the signal recovery from the sample flesh, where the reference chemical composition was measured. It is also possible to observe differences between the estimation quality and the skin type on each side of the fish. The correlation was shown to be higher for the blind side (lighter skin) compared to the ocular side (darker skin). It is worth mentioning that the outcomes of the spectral unmixing analysis are affected by which endmembers are used to model the light interaction with tissue, as well as the spectral bands used and the assumptions for modeling the scattering of light in tissue. The estimation of fat and water content using

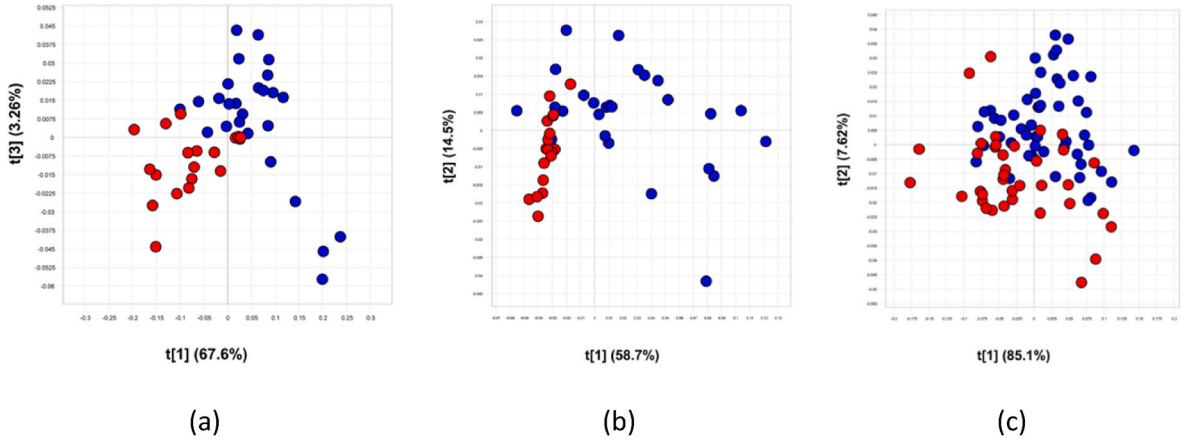

Fig. 4. Score plots for the PLS-DA modeling for the classification of MHS (red) and non-MHS (blue). (a) Ocular side, (b) Blind side, (c) Fillets. (For interpretation of the references to color in this figure legend, the reader is referred to the Web version of this article.)

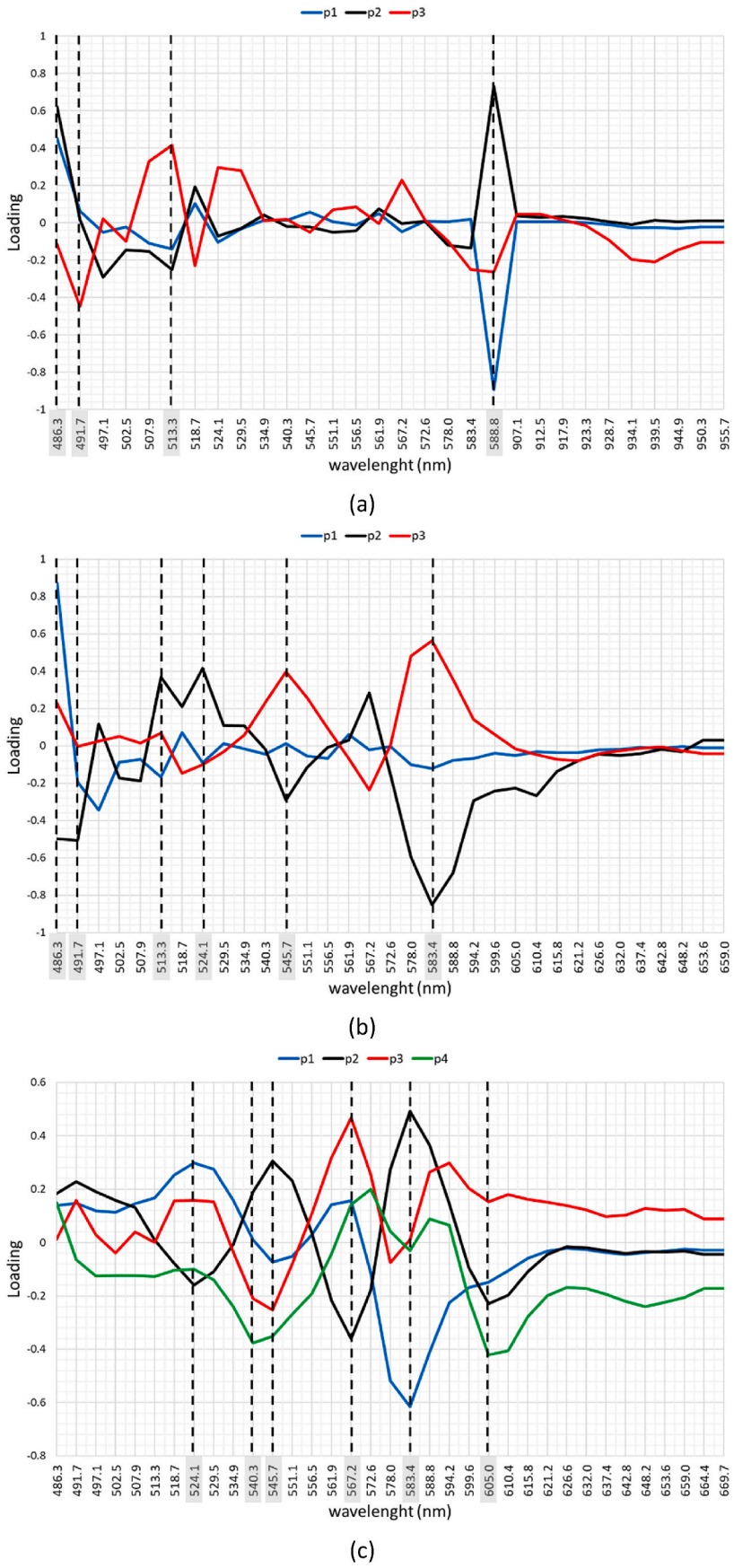

Fig. 5. Loadings for the PLS-DA models. (a) Ocular side, (b) Blind side, (c) Fillets.

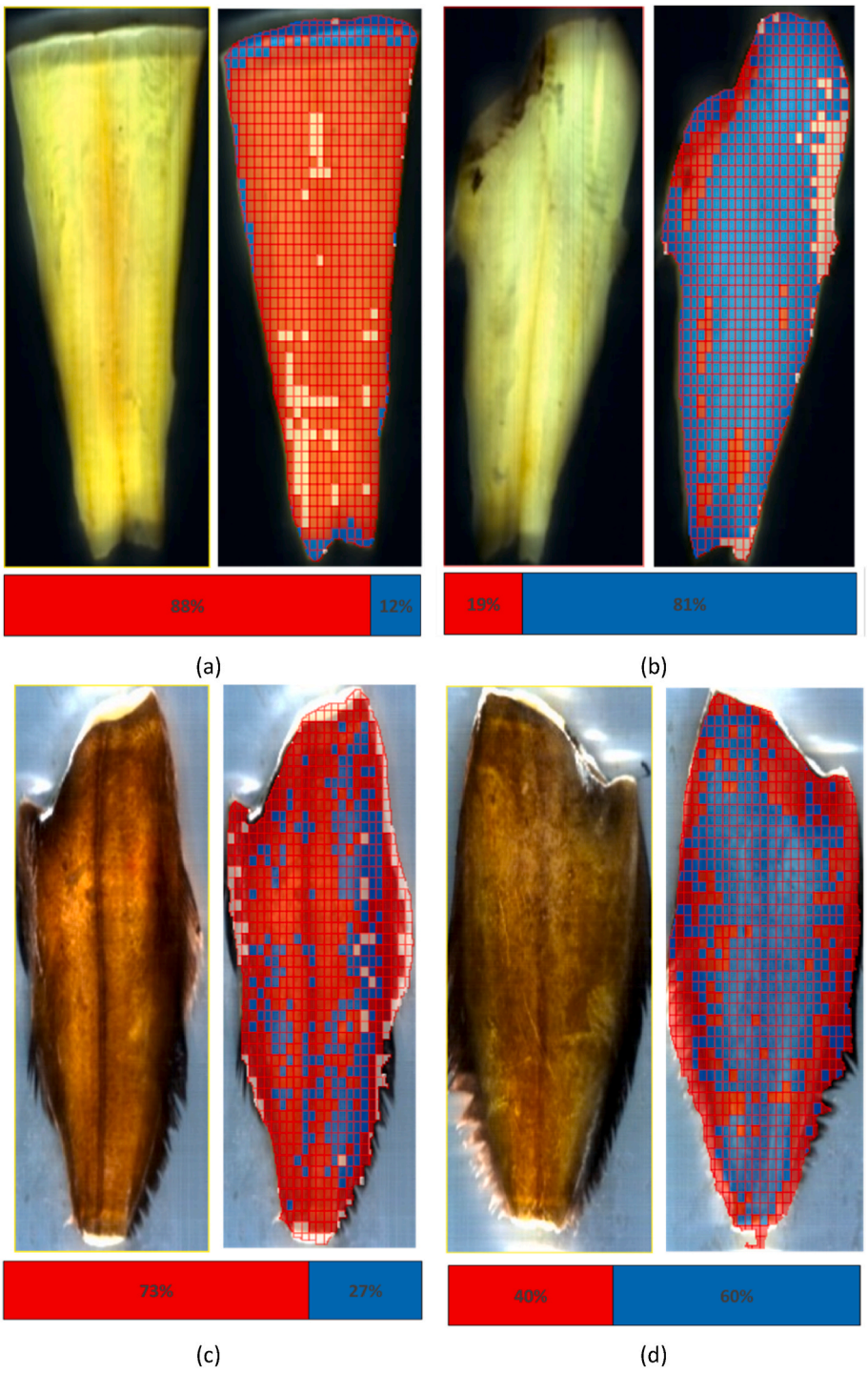

Fig. 6. Classification maps generated using the PLS-DA models over the entire sample. The red color is used to represent the class MHS, while the blue color is used for the non-MHS class. The bars below each figure indicate the percentage of superpixels assigned to each class. (a) MHS fillet (b) Non-MHS fillet (c) MHS whole fish (d) Non-MHS whole fish. (For interpretation of the references to color in this figure legend, the reader is referred to the Web version of this article.)

hyperspectral imaging and spectral unmixing may be improved using a more sophisticated model for modeling the tissue in the halibut samples, e.g., using additional endmembers to model the light interaction with the different skin types. Furthermore, according to the analysis of the chemical composition of the samples, the protein and the ash contents were shown to be relevant for differentiating between affected or not by the MHS. However, one limitation of our study is the lack of reference endmember spectra for protein and ash, which makes it impossible to perform an estimation of ash and proteins.

The second goal of the hyperspectral image analysis was to perform an automatic identification of the MHS. To this end, we used a PLS-DA for the binary classification of the samples by exploiting their spectral information. The PLS-DA classification was proven to be more accurate in fillets (with no misclassifications) compared to the data classification using whole fish hyperspectral images. However, the results on whole fish are also precise, with competitive precision and recall. The results were also improved when the spectral information from an ROI located in the loin of the sample was used, compared to the use of spectral

information from the entire sample. Identifying Greenland halibut affected by MHS before they have been filleted could benefit the industry since the cost of processing the fish affected by MHS could be avoided.

For this reason, we can conclude that hyperspectral imaging is a technology that can be used for the non-invasive identification of MHS. However, the proposed approach presents some limitations. Firstly, the PLS-DA models for each type of hyperspectral image (ocular side, blind side, and fillets) were found to be optimal using different spectral ranges. For the industrial use of this model, this means that is necessary to identify which side of the Greenland halibut is being imaged before the classification model is applied. Additionally, the interpretation of how the models were related to the information about the sample's chemical composition to perform the classification is not straightforward. Secondly, the annotations of the samples in this study were performed only using two categories: MHS and non-MHS. A more complex annotation strategy could be followed to consider the different degrees of severity of the MHS in each sample, enabling a more accurate sorting of the fish. Finally, this research was performed in a limited set of data, where only 13 samples were used to evaluate the PLS-DA models. For this reason, in future works, the identification of MHS using hyperspectral data must be proven with a larger sample size.

Finally, it should be mentioned that our experiments were carried out on Greenland halibut that were frozen and thawed before the image acquisition. This method should be evaluated in fresh fish, just after their capture and before rigor mortis, to prove its potential as a practical industrial application.

5. Conclusions

MHS is a common phenomenon that leads to economic losses for fishermen and food industry producers. To date, this syndrome has not been carefully investigated, either from the biological point of view or for the use of novel technologies for its detection. This research aimed to evaluate hyperspectral imaging as a suitable technology for the characterization and early identification of MHS. The potential advantage of hyperspectral imaging over other technologies that may also be useful for identifying MHS is to be non-contact, non-invasive, and adequate to be used in industrial conditions. In this study, we proposed two alternatives to exploit spectral information to identify MHS: the estimation of the chemical composition and the automatic classification of the samples.

The results for estimating the chemical composition using constrained spectral unmixing present some limitations. Fat estimation with a strong correlation with the reference data is possible under certain circumstances, i.e., only in fillets and the blind side images. However, the other chemical components relevant to the characterization of the MHS cannot be estimated. For that reason, additional research should be performed to improve the retrieval of the chemical composition from the spectral data to characterize the MHS.

However, detecting Greenland halibut affected by MHS was proven possible without using information about the chemical composition of the samples but using spectral data in the PLS-DA supervised classification. The results of those classifications showed a perfect classification of the hyperspectral images of the fillets. Furthermore, the classification using the whole fish (before filleting) was also accurate, with high precision and recall. The supervised classification results suggest that hyperspectral imaging could potentially be used in industrial environments to screen MHS, allowing an accurate grading of the seafood products, improving the product sorting according to their quality, and thus preventing economic losses.

CRediT authorship contribution statement

Samuel Ortega: Conceptualization, Methodology, Investigation, Software, Formal analysis, Writing – original draft. **Stein-Kato Lindberg:** Investigation, Formal analysis, Writing – original draft. **Stein Harris Olsen:** Investigation, Validation, Writing – review & editing. **Kathryn E. Anderssen:** Supervision, Data curation, Formal analysis, Writing – review & editing. **Karsten Heia:** Conceptualization, Methodology, Writing – review & editing, Project administration, Funding acquisition.

Data availability

The data that has been used is confidential.

Acknowledgments

This work was partially funded by the Research Council of Norway through the projects *SFI Digital Food Quality* [grant number 309259], and *More Efficient Utilization of Marine Resources through Multiscale Magnetic Resonance Imaging* [grant number 294805]. The authors thank Amanda Karlsen for assistance with the image acquisition, sample preparation, and initial screening.

References

Afseth, N. K., Segtnan, V. H., Marquardt, B. J., & Wold, J. P. (2005). Raman and near-infrared spectroscopy for quantification of fat composition in a complex food model system. *Applied Spectroscopy, 59*(11), 1324–1332. https://doi.org/10.1366/000370205774783304

Alasalvar, C., Miyashita, K., Shahidi, F., & Wanasundara, U. (2011). *Handbook of seafood quality, safety and health applications*. John Wiley & Sons.

Barkley, A. (2015). *Implications of developing deep-sea arctic fisheries for Greenland halibut (Reinhardtius hippoglossoides): Inshore stock connectivity and capture induced stress of ecologically important fish species* [University of Windsor] https://scholar.uwindsor.ca/etd/5429.

Careche, M., & Barroso, M. (2009). Instrumental texture measurement. In *Fishery products* (pp. 214–239). Wiley-Blackwell. https://doi.org/10.1002/9781444322668.ch9.

Careche, M., Tryggvadottir, S. V., Herrero, A., Lägel, B., Petermann, U., Schubring, R., & Nesvadba, P. (2003). Instrumental methods for measuring texture of fish. In J. B. Luten, J. Oehlenschläger, & G. Ólafsdóttir (Eds.), *Quality of fish from catch to consumer* (pp. 189–200). Wageningen Academic Publishers. https://doi.org/10.3920/978-90-8686-510-9.

Cheng, J.-H., Sun, D.-W., & Wei, Q. (2017). Enhancing visible and near-infrared hyperspectral imaging prediction of TVB-N level for fish fillet freshness evaluation by filtering optimal variables. *Food Analytical Methods, 10*(6), 1888–1898. https://doi.org/10.1007/s12161-016-0742-9

Cheng, J.-H., Sun, D.-W., Zeng, X.-A., & Pu, H.-B. (2014). Non-destructive and rapid determination of TVB-N content for freshness evaluation of grass carp (Ctenopharyngodon idella) by hyperspectral imaging. *Innovative Food Science & Emerging Technologies, 21*, 179–187. https://doi.org/10.1016/j.ifset.2013.10.013

Dixit, Y., & Reis, M. M. (2023). Hyperspectral imaging for assessment of total fat in salmon fillets: A comparison between benchtop and snapshot systems. *Journal of Food Engineering, 336*, Article 111212. https://doi.org/10.1016/j.jfoodeng.2022.111212

Dwyer, K. S., Treble, M. A., & Campana, S. E. (2016). Age and growth of Greenland halibut (Reinhardtius hippoglossoides) in the Northwest Atlantic: A changing perception based on bomb radiocarbon analyses. *Fisheries Research, 179*, 342–350. https://doi.org/10.1016/j.fishres.2016.01.016

ElMasry, G., & Wold, J. P. (2008). High-speed assessment of fat and water content distribution in fish fillets using online imaging spectroscopy. *Journal of Agricultural and Food Chemistry, 56*(17), 7672–7677. https://doi.org/10.1021/jf801074s

Fiskeridirektoratet. (2020). *Economic and biological figures from Norwegian fisheries 2020*. https://www.fiskeridir.no/English/Fisheries/Statistics/Economic-and-biological-key-figures.

Heia, K., Sivertsen, A. H., Stormo, S. K., Elvevoll, E., Wold, J. P., & Nilsen, H. (2007). Detection of nematodes in cod (Gadus morhua) fillets by imaging spectroscopy. *Journal of Food Science, 72*(1), E011–E015. https://doi.org/10.1111/j.1750-3841.2006.00212.x

Herrmann, B., Sistiaga, M., Larsen, R. B., Nielsen, K. N., & Grimaldo, E. (2013). Understanding sorting grid and codend size selectivity of Greenland halibut (Reinhardtius hippoglossoides). *Fisheries Research, 146*, 59–73. https://doi.org/10.1016/j.fishres.2013.04.004

Jepsen, S. M., Pedersen, H. T., & Engelsen, S. B. (1999). Application of chemometrics to low-field1H NMR relaxation data of intact fish flesh. *Journal of the Science of Food and Agriculture, 79*(13), 1793–1802. https://doi.org/10.1002/(SICI)1097-0010(199910)79:13<1793::AID-JSFA437>3.0.CO;2-S

Khodabux, K., Lomelette, M., Jhaumeerlaulloo, S., Ramasami, P., & Rondeau, P. (2007). Chemical and near-infrared determination of moisture, fat and protein in tuna fishes. *Food Chemistry, 102*(3), 669–675. https://doi.org/10.1016/j.foodchem.2006.05.057

Khoshnoudi-Nia, S., & Moosavi-Nasab, M. (2019). Prediction of various freshness indicators in fish fillets by one multispectral imaging system. *Scientific Reports, 9*(1), Article 14704. https://doi.org/10.1038/s41598-019-51264-z

Khoshtaghaza, M. H., Khojastehnazhand, M., Mojaradi, B., Goodarzi, M., & Saeys, W. (2016). Texture quality analysis of rainbow trout using hyperspectral imaging method. *International Journal of Food Properties, 19*(5), 974–983. https://doi.org/10.1080/10942912.2015.1042111

Lefevre, F., & Bugeon, J. (2008). Biological basis of fish quality. *Sciences des Aliments, 28* (4–5), 365–377. https://doi.org/10.3166/sda.28.365-377

Lei, T., Lin, X.-H., & Sun, D.-W. (2019). Rapid classification of commercial Cheddar cheeses from different brands using PLSDA, LDA and SPA–LDA models built by hyperspectral data. *Journal of Food Measurement and Characterization, 13*(4), 3119–3129. https://doi.org/10.1007/s11694-019-00234-0

Liu, D., Zeng, X.-A., & Sun, D.-W. (2013). NIR spectroscopy and imaging techniques for evaluation of fish quality—a review. *Applied Spectroscopy Reviews, 48*(8), 609–628. https://doi.org/10.1080/05704928.2013.775579

Martinsdttir, E., Schelvis, R., Hyldig, G., & Sveinsdttir, K. (2009). Sensory evaluation of seafood: Methods. In *Fishery products* (pp. 425–443). Wiley-Blackwell. https://doi.org/10.1002/9781444322668.ch20.

Ma, J., Sun, D.-W., Nicolai, B., Pu, H., Verboven, P., Wei, Q., & Liu, Z. (2019). Comparison of spectral properties of three hyperspectral imaging (HSI) sensors in evaluating main chemical compositions of cured pork. *Journal of Food Engineering, 261*, 100–108. https://doi.org/10.1016/j.jfoodeng.2019.05.024

Meyers, T. R., Bentz, C., Ferguson, J., Stewart, D., Starkey, N., & Burton, T. (2019). *Diseases of wild and cultured fishes in Alaska*. Fish Pathology Laboratories: Alaska Department of Fish and Game.

Nilsen, H. A., & Heia, K. (2009). VIS/NIR spectroscopy. In *Fishery products* (pp. 89–104). Wiley-Blackwell. https://doi.org/10.1002/9781444322668.ch5.

Nollet, L. M. L., & Toldrá, F. (2009). *Handbook of seafood and seafood products analysis*. CRC Press.

Olsen, S. H., Sørensen, N. K., Larsen, R., Elvevoll, E. O., & Nilsen, H. (2008). Impact of pre-slaughter stress on residual blood in fillet portions of farmed Atlantic cod (Gadus morhua) — measured chemically and by Visible and Near-infrared spectroscopy. *Aquaculture, 284*(1–4), 90–97. https://doi.org/10.1016/j.aquaculture.2008.07.042

Ortega, S., Lindberg, S.-K., Anderssen, K. E., & Heia, K. (2022). Perspective chapter: Hyperspectral imaging for the analysis of seafood. In D. J. Y. Huang (Ed.), *Hyperspectral imaging - a perspective on recent advances and applications*. IntechOpen. https://doi.org/10.5772/intechopen.108726.

Özdoğan, G., Lin, X., & Sun, D.-W. (2021). Rapid and noninvasive sensory analyses of food products by hyperspectral imaging: Recent application developments. *Trends in Food Science & Technology, 111*, 151–165. https://doi.org/10.1016/j.tifs.2021.02.044

Petricorena, Z. C. (2015). Chemical composition of fish and fishery products. In P. C. K. Cheung (Ed.), *Handbook of food chemistry* (pp. 1–28). Springer Berlin Heidelberg. https://doi.org/10.1007/978-3-642-41609-5_12-1.

Pope, R. M., & Fry, E. S. (1997). Absorption spectrum (380–700 nm) of pure water II Integrating cavity measurements. *Applied Optics, 36*(33), 8710. https://doi.org/10.1364/AO.36.008710

Pu, Y.-Y., Sun, D.-W., Buccheri, M., Grassi, M., Cattaneo, T. M. P., & Gowen, A. (2019). Ripeness classification of bananito fruit (musa acuminata, AA): A comparison study of visible spectroscopy and hyperspectral imaging. *Food Analytical Methods, 12*(8), 1693–1704. https://doi.org/10.1007/s12161-019-01506-7

Saha, D., & Manickavasagan, A. (2021). Machine learning techniques for analysis of hyperspectral images to determine quality of food products: A review. *Current Research in Food Science, 4*, 28–44. https://doi.org/10.1016/j.crfs.2021.01.002

Schober, P., Boer, C., & Schwarte, L. A. (2018). Correlation coefficients. *Anesthesia & Analgesia, 126*(5), 1763–1768. https://doi.org/10.1213/ANE.0000000000002864

Sivertsen, A. H., Chu, C.-K., Wang, L.-C., Godtliebsen, F., Heia, K., & Nilsen, H. (2009). Ridge detection with application to automatic fish fillet inspection. *Journal of Food Engineering, 90*(3), 317–324. https://doi.org/10.1016/j.jfoodeng.2008.06.035

Sivertsen, A. H., Heia, K., Hindberg, K., & Godtliebsen, F. (2012). Automatic nematode detection in cod fillets (Gadus morhua L.) by hyperspectral imaging. *Journal of Food Engineering, 111*(4), 675–681. https://doi.org/10.1016/j.jfoodeng.2012.02.036

Sivertsen, A. H., Kimiya, T., & Heia, K. (2011). Automatic freshness assessment of cod (Gadus morhua) fillets by Vis/Nir spectroscopy. *Journal of Food Engineering, 103*(3), 317–323. https://doi.org/10.1016/j.jfoodeng.2010.10.030

Skjelvareid, M. H., Heia, K., Olsen, S. H., & Stormo, S. K. (2017). Detection of blood in fish muscle by constrained spectral unmixing of hyperspectral images. *Journal of Food Engineering, 212*, 252–261. https://doi.org/10.1016/j.jfoodeng.2017.05.029

Sogn-Grundvåg, G., & Zhang, D. (2021). *Auction versus direct sale: The effect of buyers and sellers on prices. European review of agricultural economics*. https://doi.org/10.1093/erae/jbab051

Sogn-Grundvåg, G., Zhang, D., Henriksen, E., Joensen, S., Bendiksen, B.-I., & Hermansen, Ø. (2022). Fishing tactics and fish quality: The case of the coastal fishery for Atlantic cod in Norway. *Fisheries Research, 246*, Article 106167. https://doi.org/10.1016/j.fishres.2021.106167

Sydeman, W. J., Piatt, J. F., Thompson, S. A., García-Reyes, M., Hatch, S. A., Arimitsu, M. L., Slater, L., Williams, J. C., Rojek, N. A., Zador, S. G., & Renner, H. M. (2017). Puffins reveal contrasting relationships between forage fish and ocean climate in the North Pacific. *Fisheries Oceanography, 26*(4), 379–395. https://doi.org/10.1111/fog.12204

Tsai, B. K., Allen, D. W., Hanssen, L. M., Wilthan, B., & Zeng, J. (2008). In Z.-H. Gu, & L. M. Hanssen (Eds.), *A comparison of optical properties between solid PTFE (Teflon) and (low density) sintered PTFE*. 70650Y. https://doi.org/10.1117/12.798138.

Wang, X., Shan, J., Han, S., Zhao, J., & Zhang, Y. (2019). Optimization of fish quality by evaluation of total volatile basic nitrogen (TVB-N) and texture profile analysis (TPA) by near-infrared (NIR) hyperspectral imaging. *Analytical Letters, 52*(12), 1845–1859. https://doi.org/10.1080/00032719.2019.1571077

Wang, Q. X., Su, L. H., Zou, J., Chen, N. X., Wu, T., & Yang, L. (2021). Research on hardness detection method of crisped grass carp based on visible - near infrared hyperspectral technology. *Journal of Physics: Conference Series, 1757*(1), Article 012002. https://doi.org/10.1088/1742-6596/1757/1/012002

Washburn, K. E., Stormo, S. K., Skjelvareid, M. H., & Heia, K. (2017). Non-invasive assessment of packaged cod freeze-thaw history by hyperspectral imaging. *Journal of Food Engineering, 205*, 64–73. https://doi.org/10.1016/j.jfoodeng.2017.02.025

Wilson, R. H., Nadeau, K. P., Jaworski, F. B., Tromberg, B. J., & Durkin, A. J. (2015). Review of short-wave infrared spectroscopy and imaging methods for biological tissue characterization. *Journal of Biomedical Optics, 20*(3), Article 030901. https://doi.org/10.1117/1.JBO.20.3.030901

Wold, J. P., Johansen, I.-R., Haugholt, K. H., Tschudi, J., Thielemann, J., Segtnan, V. H., Narum, B., & Wold, E. (2006). Non-contact transflectance near infrared imaging for representative on-line sampling of dried salted coalfish (bacalao). *Journal of Near Infrared Spectroscopy, 14*(1), 59–66. https://doi.org/10.1255/jnirs.587

Wu, D., & Sun, D.-W. (2013). Advanced applications of hyperspectral imaging technology for food quality and safety analysis and assessment: A review — Part I: Fundamentals. *Innovative Food Science & Emerging Technologies, 19*, 1–14. https://doi.org/10.1016/j.ifset.2013.04.014

Yu, H.-D., Qing, L.-W., Yan, D.-T., Xia, G., Zhang, C., Yun, Y.-H., & Zhang, W. (2021). Hyperspectral imaging in combination with data fusion for rapid evaluation of tilapia fillet freshness. *Food Chemistry, 348*, Article 129129. https://doi.org/10.1016/j.foodchem.2021.129129

Zhang, H., Zhang, S., Chen, Y., Luo, W., Huang, Y., Tao, D., Zhan, B., & Liu, X. (2020). Non-destructive determination of fat and moisture contents in Salmon (Salmo salar) fillets using near-infrared hyperspectral imaging coupled with spectral and textural features. *Journal of Food Composition and Analysis, 92*, Article 103567. https://doi.org/10.1016/j.jfca.2020.103567

Zhu, F., Zhang, H., Shao, Y., He, Y., & Ngadi, M. (2014). Mapping of fat and moisture distribution in atlantic salmon using near-infrared hyperspectral imaging. *Food and Bioprocess Technology, 7*(4), 1208–1214. https://doi.org/10.1007/s11947-013-1228-z